Published in final edited form as:
Dalton Trans. 2011 March 14; 40(10): 2234–2241. doi:10.1039/c0dt01036g.

Spectroscopic and computational characterization of Cu^{II}–OOR (R = H or cumyl) complexes bearing a Me_6-tren ligand†

Yu Jin Choi[a], **Kyung-Bin Cho**[b], **Minoru Kubo**[c], **Takashi Ogura**[c], **Kenneth D. Karlin**[b,d], **Jaeheung Cho**[a], and **Wonwoo Nam**[a,b]

Kenneth D. Karlin: karlin@jhu.edu; Jaeheung Cho: jaeheung@ewha.ac.kr; Wonwoo Nam: wwnam@ewha.ac.kr

[a]Department of Chemistry and Nano Science, Ewha Womans University, Seoul, 120-750, Korea; Fax: +82 2 3277 4441; Tel: +82 2 3277 4108

[b]Department of Bioinspired Science, Ewha Womans University, Seoul, 120-750, Korea

[c]Picobiology Institute, Graduate School of Life Science, University of Hyogo, Hyogo, 678-1297, Japan

[d]Department of Chemistry, Johns Hopkins University, Baltimore, MD, USA, 21218

Abstract

A copper(II)–hydroperoxo complex, $[Cu(Me_6\text{-tren})(OOH)]^+$ (**2**), and a copper(II)–cumylperoxo complex, $[Cu(Me_6\text{-tren})(OOC(CH_3)_2Ph)]^+$ (**3**), were synthesized by reacting $[Cu(Me_6\text{-tren})(CH_3CN)]^{2+}$ (**1**) with H_2O_2 and cumyl-OOH, respectively, in the presence of triethylamine. These intermediates, **2** and **3**, were successfully characterized by various physicochemical methods such as UV-vis, ESI-MS, resonance Raman and EPR spectroscopies, leading us to propose structures of the Cu(II)–OOR species with a trigonal-bipyramidal geometry. Density functional theory (DFT) calculations provided geometric and electronic configurations of **2** and **3**, showing trigonal bipyramidal copper(II)–OOR geometries. These copper(II)–hydroperoxo and –cumylperoxo complexes were inactive in electrophilic and nucleophilic oxidation reactions.

Introduction

The generation and study of metal–peroxo complexes has a considerable history, as the employment of such species is of interest to a number of disciplines, including organic oxidation processes occurring in chemical or biochemical settings.[1–3] The latter field captures the interest of a very large (bio)chemical research community, since metalloenzymes, especially those containing heme, non-heme iron and copper, bind molecular oxygen and then utilize metal–peroxo and metal–hydroperoxo species (or species derived from them) to effect biochemical substrate oxidations.[1,4–7]

Our own interests include coordination chemistry studies on copper–dioxygen complexes and derived species, with the primary goal of establishing fundamental aspects of adduct formation, structure–spectroscopic correlations and substrate–reactivity patterns.[8–11] The studies are inspired by the diverse array of reactions mediated at protein active sites, reversible binding of O_2, insertion of O-atom(s) into substrates by oxygenases, and

†Electronic supplementary information (ESI) available: ESI-MS of **1** and *xyz* coordinates, selected geometrical parameters and overlay figure from the computational calculations. CCDC reference number 775689. For ESI and crystallographic data in CIF or other electronic format see DOI: 10.1039/c0dt01036g

Correspondence to: Jaeheung Cho, jaeheung@ewha.ac.kr; Wonwoo Nam, wwnam@ewha.ac.kr.

dehydrogenation reactions mediated by copper oxidases.[12] Protein active-site environments may possess one, two or three proximate copper ions.[12–16]

Copper–peroxo species are now well established to occur in the blood O_2-carrier proteins hemocyanins, which bind O_2 *via* formation of binuclear Cu^{II}–(O_2^{2-})–Cu^{II} complexes, as do monooxygenase tyrosinases.[13,14,17] A copper–peroxo species is also strongly implicated at the trinuclear active center in 'blue' multicopper oxidases, with a $Cu^{I}Cu^{II}_2$–(O_2^{2-}) formulation[18] as supported by crystallographic studies.[19] Protonation to give a hydroperoxo ($^{-}$OOH) intermediate, or proton-induced peroxo complex reduction to water, follows.[18,20]

As implied, all oxygenases and oxidases utilize molecular oxygen; thus, O_2-derived (*i.e.*, reduced) active species must begin by reaction with a copper(I) center to produce a cupric–superoxo (*i.e.*, Cu^{II}–$O_2^{\bullet-}$) initial adduct (Scheme 1).[8,21,22] Significantly, only one example of a putative protein Cu^{II}–$O_2^{\bullet-}$ species is known (see below).[23] In fact, advances in synthetic model chemistry have provided considerable information, in that there are now well characterized O_2-adducts or derived species representing both mono- (Scheme 1) and dicopper entities. For the former case, both end-on η^1-($O_2^{\bullet-}$) copper(II) complexes[21,22] and a side-on η^2-($O_2^{\bullet-}$) copper(II) complex[24] have been structurally and spectroscopically characterized. With a strongly donating anionic ligand for copper; Tolman and coworkers[25] described a side-on η^2-(O_2^{2-}) copper(III) complex (Scheme 1). Mononuclear Cu^{II}–hydroperoxo complexes have been studied;[11,26–36] they are formed either from addition of H_2O_2/base to a precursor copper(II) complex, or in one instance, *via* reaction of a ligand–Cu^{II}–($O_2^{\bullet-}$) complex with a phenol as an electron/proton donor.[35] Masuda and coworkers[26] were able to obtain an X-ray structure employing a tripodal tetradentate ligand which also carries groups capable of H-bonding to the coordinated $^{-}$OOH ligand (see the structure below).

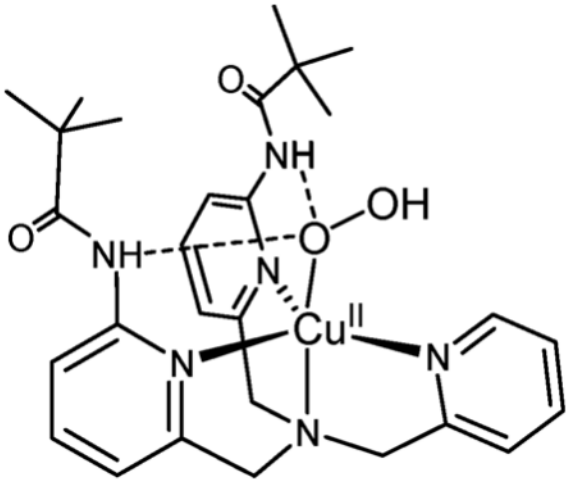

Tripodal tetradentate ligands have been very popular in studying dioxygen reactivity by ligand–copper(I) complexes. These include tris(2-pyridylmethyl)amine (TMPA) and analogues or derivatives.[9,30] This is also true for the classic tripodal tren ligand, tris(2-aminoethyl)amine; tren derivatives and copper–dioxygen chemistry have been especially studied by the research groups of Schindler[21,37–39] and Suzuki,[40] providing extensive insights into ligand–Cu^{I}/O_2 reactivity and kinetics, as well as formation of Cu^{II}–($O_2^{\bullet-}$) species (with an as-mentioned X-ray structure),[21] and dicopper(II)–peroxo species, the latter also with an X-ray structure known from Suzuki.[40]

Notably, copper–hydroperoxo or –alkylperoxo species generated using tren derivatives do not appear in the literature. Thus, in this report, we have added to the base of compounds studied for this category of compounds. Using Me_6-tren (tris(*N*,*N*′-dimethylaminoethyl)amine), we describe the synthesis and detailed characterization of a hydroperoxo and cumylperoxo complex with Me_6-tren (see the structure below).

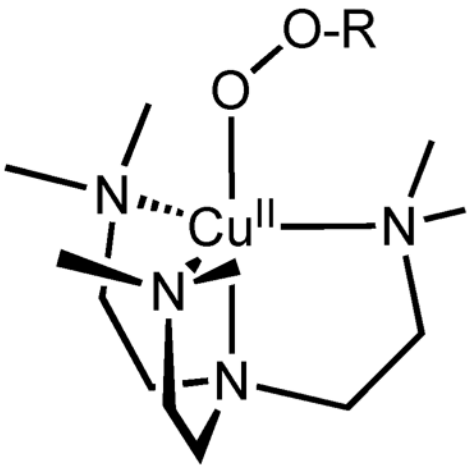

In fact, there is currently an increase of research effort in the community to elucidate reactivity trends for Cu^{II}–(OOH) *vs.* Cu^{II}–($O_2^{\bullet-}$) species. This is due to the considerable literature discussion[35,41,42] concerning which entity is responsible for initial hydrogen-atom (H-atom) abstraction reaction occurring in the closely related copper enzymes dopamine β-monooxygenase (DβM) and peptidylglycine α-hydroxylating monooxygenase (PHM). These possess well-separated (~11 Å) copper ions; however, biochemical studies indicate the active site is at one of the copper ions (the so-called Cu_M site, possessing $His_2Met\ N_2S$ ligation).[43] An X-ray structure of a PHM derivative displays a presumed Cu^{II}–($O_2^{\bullet-}$) entity with end-on η^1-coordination.[23] Such a cupric superoxo complex capable of effecting an enzymatic substrate hydroxylation *via* initial H-atom abstraction has drawn experimental[43] and theoretical[44] support. Yet, in synthetic chemistry there is so far only one example[45] where a Cu^{II}–($O_2^{\bullet-}$) entity is shown to be capable of H-atom abstraction. A Cu^{II}–OOH species would derive from an electron–proton downstream reaction, and some of us have published some examples where copper–hydroperoxo complexes appear to initiate H-atom abstraction and oxygen atom transfer reactions.[32,35,36,46] In addition, studies of Cu^{II}–OOR (R = acyl, alkyl) species and their reactivity have contributed to our basic understanding in the field.[47–51] From a Cu^{II}–OOR species, a thus far highly elusive high-valent copper–oxo species (“cupryl”, Scheme 1) may form *via* O–O cleavage chemistry, and this is likely a relevant species somewhere on the path of Cu^I/O_2 reaction to species involved in enzyme-like C–H substrate oxidation chemistry.[10,36,41,51–54] Thus, extensive investigations to fully elucidate the chemistry of Cu^{II}–($O_2^{\bullet-}$) and Cu^{II}–OOR moieties are required.

Results and discussion

Copper(II) precursor complex

The starting material, $[Cu(Me_6\text{-tren})(CH_3CN)](ClO_4)_2$ (**1**-$(ClO_4)_2$), was prepared by reacting $Cu(ClO_4)_2{\cdot}6H_2O$ and Me_6-tren in CH_3CN. The UV-visible spectrum of **1** in CH_3CN exhibits one broad band at ~850 nm (ε = 500 $M^{-1}\ cm^{-1}$) (Fig. 2a). The electrospray ionization mass spectrum (ESI-MS) of **1** shows intense isotope envelopes at a mass-to-charge (*m*/*z*) of 392.1 for $[Cu(Me_6\text{-tren})(ClO_4)]^+$ (see Fig. S1[†]). After numerous attempts to

determine the X-ray structure of the starting material, suitable crystals were obtained by the addition of $NaBPh_4$ to the solution of **1**-$(ClO_4)_2$.

The crystal structure of the cation part of **1**-$(BPh_4)_2$ is shown in Fig. 1, and selected bond distances and angles are listed in Table 1. Complex **1** has a five-coordinated Cu(II) ion with four nitrogens of the Me_6-tren ligand and one nitrogen of CH_3CN coordinating to the free axial position. The Cu(II) geometry is best described as trigonal bipyramidal (τ = 0.95), similar to that found in [Cu(Me_6-tren)(H_2O)]$^{2+}$.[55,56]

Copper(II)–hydroperoxo complex and characterization

The copper(II)–hydroperoxo complex, [Cu(Me_6-tren)(OOH)]$^+$ (**2**), was prepared by adding 10 equiv of H_2O_2 to a reaction solution containing **1** in the presence of 2 equiv triethylamine (TEA) in a solvent mixture of CH_3CN and CH_3OH (1:1) at 0 °C; the color of the solution changed from blue to green (Scheme 2). A UV-vis spectrum of **2** shows an intense band at 375 nm (ε = 1250 M^{-1} cm^{-1}) and two weak bands at 680 (ε = 220 M^{-1} cm^{-1}) and 840 nm (ε = 270 M^{-1} cm^{-1}) (Fig. 2a), which is similar to those of the previously reported copper(II)–hydroperoxo complexes.[26,29,57,58] The former band has been assigned as the LMCT band of the Cu^{II}–OOH species, and the latter two bands have been assigned as the d–d transition bands of the Cu(II) ion with a trigonal-bipyramidal geometry.[29]

The ESI-MS of **2** exhibits a prominent ion peak at *m*/*z* of 326.1 (Fig. 2b), whose mass and isotope distribution pattern correspond to [Cu(Me_6-tren)(OOH)]$^+$ (**2**-^{16}O) (calculated *m*/*z* of 326.2). When the reaction was carried out with isotopically labeled $H_2{}^{18}O_2$, a mass peak corresponding to [Cu(Me_6-tren)($^{18}O^{18}OH$)]$^+$ (**2**-^{18}O) appeared at *m*/*z* of 330.1 (calculated *m*/*z* of 330.2) (Fig. 2b). The shift in four mass units on substitution of ^{16}O with ^{18}O proves that **2** contains an O_2 unit.

The resonance Raman spectrum of **2** was collected using 407 nm excitation in a solvent mixture of CH_3CN and CH_3OH (1:1) at − 20 °C. **2** prepared with $H_2{}^{16}O_2$ exhibits two isotopically sensitive bands at 846 and 509 cm^{-1} that shift to 798 and 484 cm^{-1}, respectively, in samples of **2** prepared with $H_2{}^{18}O_2$ (Fig. 2c). The higher-energy feature (846 cm^{-1}) with $^{16}\Delta - {}^{18}\Delta$ value of 48 cm^{-1} ($^{16}\Delta - {}^{18}\Delta$ (calcd) = 48 cm^{-1}) is ascribed to the O–O stretching vibration of the hydroperoxo ligand, and the lower-energy feature (509 cm^{-1}) is assigned to the Cu–O stretching vibration ($^{16}\Delta - {}^{18}\Delta$ = 25 $cm^{-1;}$ $^{16}\Delta - {}^{18}\Delta$ (calcd) = 23 cm^{-1}).

The electron paramagnetic resonance (EPR) spectrum of a frozen solution of **2** measured at 4.3 K is typical of trigonal-bipyramidal Cu(II) complexes, having a “reverse” axial appearance with $g_\perp > g_\parallel \sim 2.0$ and $A_\perp$ = 60–100 × 10^{-4} cm^{-1} (Fig. 2d).[59–63] The $g_\perp$ (2.20), $g_\parallel$ (2.00), $A_\perp$ (87 G), and $A_\parallel$ (83 G) values are comparable to those of the previously reported Cu(II) complexes with a trigonal-bipyramidal geometry.

Copper(II)–cumylperoxo complex and characterization

The copper(II)–cumylperoxo complex, [Cu(Me_6-tren)(OOC-$(CH_3)_2$Ph)]$^+$ (**3**), was generated by adding 5 equiv of cumene hydroperoxide (cumyl-OOH) to the solution of **1** in the presence of 2 equiv triethylamine in CH_3CN at 25 °C; the color of the solution changed from blue to green (Scheme 2). Spectroscopic properties of **3** are similar to those of **2**. The UV-visible spectrum of **3** in CH_3CN at 25 °C exhibits weak bands at 440 (ε = 280 M^{-1} cm^{-1}), 680 (ε = 250 M^{-1} cm^{-1}) and 787 nm (ε = 300 M^{-1} cm^{-1}) (Fig. 3a).

†Electronic supplementary information (ESI) available: ESI-MS of **1** and *xyz* coordinates, selected geometrical parameters and overlay figure from the computational calculations. CCDC reference number 775689. For ESI and crystallographic data in CIF or other electronic format see DOI: 10.1039/c0dt01036g

The ESI-MS of **3** in CH_3CN at 25 °C shows a prominent ion peak at *m*/*z* of 444.0 (Fig. 3b), whose mass and isotope distribution pattern correspond to $[Cu(Me_6\text{-tren})(OOC(CH_3)_2Ph)]^+$ (**3**-^{16}O) (calculated *m*/*z* of 444.2). When the reaction was carried out with isotopically labeled cumyl-$^{18}O^{18}OH$, a mass peak corresponding to $[Cu(Me_6\text{-tren})(^{18}O^{18}OC(CH_3)_2Ph)]^+$ (**3**-^{18}O) appeared at *m*/*z* of 448.0 (calculated *m*/*z* of 448.2) (Fig. 3b, inset). The four mass unit increase upon substitution of ^{16}O with ^{18}O indicates that **3** contains an O_2 unit.

The resonance Raman spectrum of **3** was collected using 442 nm excitation in CH_3CN at −20 °C. **3** prepared with cumyl-OOH exhibits two isotopically sensitive bands at 887 and 839 cm^{-1}, which shift to 805 cm^{-1} in samples of **3** prepared with cumyl-$^{18}O^{18}OH$ (Fig. 3c). Such a band shift has been observed in copper(II)–alkylperoxo and iron(II)–alkylperoxo complexes,[51,64] and these bands have been assigned to the ν(O–O) mode.

The EPR spectrum of a frozen CH_3CN solution of **3** measured at 4.3 K shows a “reverse” axial appearance as shown in **2**, suggesting a trigonal-bipyramidal geometry for the Cu(II) ion. The $g_\perp$ (2.19), $g_\parallel$ (2.00), $A_\perp$ (77 G), and $A_\parallel$ (87 G) values are comparable to those of **2**.

Density Functional Theory results

In order to gauge the reliability of the calculations, structural comparisons were made between the crystal structure of **1** and that calculated by density functional theory (DFT).[65] The root mean square (RMS) deviation was calculated to be 0.13 Å (geometries are given in Table 1, Fig. 4 and Fig. S2†). Since some differences are expected when comparing gas-phase calculated structures with crystal forms, the structural quality of the calculations was deemed acceptable, and gave credibility to the subsequent calculations where no crystal structures are available. The Cu–peroxide geometries obtained are, as expected, of the end-on η^1 type with the metal ligand atoms in a trigonal bipyramidal fashion, with $\tau = 0.85$ for both **2** and **3** (Fig. 4), in agreement with the EPR spectroscopic results described above. For **3**, there are three possible isomers of the structure, where the phenyl ring position can be interchanged with any of the two cumene methyl positions. However, the isomers are virtually degenerate in energy, with very little differences in the core geometrical and spin parameters (hence, we only present one of them here, **3a**, and defer the other two to ESI). The O–O bond is calculated to be 1.52 Å in both **2** and **3a**. This may be compared to that observed for Masuda’s copper(II)–hydroperoxo complex (*vide supra*) (1.460 Å)[26] and a structurally characterized Fujisawa/Kitajima copper(II)–cumylperoxo complex with pyrazolylborate ligand (1.460 Å for both structures).[47,49] It is also in line with what is found in calculations of protonated Compound 0 in P450 system models.[66]

Frequency calculations were done to check that the optimized structures were indeed in a ground state. These calculations, however, also produce Raman frequencies that can be compared to the experimentally observed ones. The nearest calculated frequencies to the experimentally determined 846 and 509 cm^{-1} for **2** (*vide supra*) were found to be at 854 and 489 cm^{-1}, indeed corresponding to the O–O and O–Cu bond stretching frequencies, respectively. For **3**, experiments found two bands at 887 and 839 cm^{-1}, that shift to 805 cm^{-1} when using ^{18}O. The calculations indeed found a frequency at 845 cm^{-1} in **3a** (the isomer shown on Fig. 4) that corresponds to the O–O bond stretching, while in the other two isomers, this frequency has shifted to 857 and 855 cm^{-1}. No other frequencies near 887 cm^{-1} exhibited vibrations involving the oxygens. Hence, recognizing the crude level of calculations for spectroscopic assignments, we tentatively suggest that the experimentally observed two peaks are due to the existence of structural isomers, which collapses to one peak when the heavier (and less sensitive) ^{18}O is used. Further, more specialized, calculations may be necessary to identify the origin of the two bands more accurately.

Spin density distribution calculations show that the Cu ion retains about half a radical in the $S = \frac{1}{2}$ state, while the rest is distributed between the coordinating ligand atoms (Table 2). This is indicative of an unpaired electron occupying the $\sigma^*_{z^2}$ orbital, which is mainly distributed along the axial direction, as visualized in Fig. 5.

Reactivity

The reactivity of **2** and **3** was investigated with respective to potential electrophilic and nucleophilic reactions. First, the electrophilic character of **2** and **3** was tested in the oxidation of thioanisole and cyclohexene. Upon addition of substrates to a solution of **2** in a solvent mixture of CH_3CN and CH_3OH (1:1) at 0 °C and **3** in CH_3CN at 25 °C, **2** and **3** remained intact without showing any absorption spectral changes. The nucleophilic character of **2** and **3** was also investigated in aldehyde deformylation with cyclohexane carboxaldehyde and 2-phenylpropionaldehyde, and no spectral changes were observed. Further, product analysis of the reaction solutions revealed that no oxidized products were formed in these reactions. These results demonstrate that **2** and **3** are not capable of conducting electrophilic and nucleophilic oxidation reactions under the reaction conditions.

Conclusions

A copper(II)–hydroperoxo complex, $[Cu(Me_6\text{-tren})(OOH)]^+$ (**2**), and a copper(II)–cumylperoxo complex, $[Cu(Me_6\text{-tren})(OOC(CH_3)_2Ph)]^+$ (**3**), were generated and characterized by various spectroscopic methods. DFT calculations successfully reproduced the structure of the obtained crystal structure of $[Cu(Me_6\text{-tren})(CH_3CN)]^{2+}$ (**1**), lending credibility to the calculated structure of **2** and **3**. Calculated Raman frequencies also show good agreement with experiments. The intermediates, **2** and **3**, were inactive in electrophilic and nucleophilic oxidation reactions. These findings from the combined experimental and theoretical studies provide important fundamental information in the understanding of the nature of intermediates possibly involved in O_2-activating Cu enzymes such as DβM and PHM.

Experimental

General

All chemicals obtained from Aldrich Chemical Co. were the best available purity and used without further purification unless otherwise indicated. Solvents were dried according to published procedures and distilled under Ar prior to use.[67] $H_2{}^{18}O_2$ (90% ^{18}O-enriched, 2% $H_2{}^{18}O_2$ in water) and $^{18}O_2$ (95% ^{18}O-enriched) were purchased from ICON Services Inc. (Summit, NJ, USA). ^{18}O-Labeled cumene hydroperoxide (70% and 90% ^{18}O-enriched) was prepared by the reported method[68] and used in ESI-MS (70% ^{18}O-enriched) and resonance Raman (90% ^{18}O-enriched) studies. Me_6-tren (tris(*N*,*N*′-dimethylaminoethyl)amine) was prepared according to a published procedure.[69] $[Cu(Me_6\text{-tren})(CH_3CN)](ClO_4)_2$ was prepared by reacting $Cu(ClO_4)_2{\cdot}6H_2O$ (0.19 g, 0.50 mmol) with Me_6-tren (0.12 g, 0.50 mmol) in CH_3CN (3 mL). The mixture was stirred for several hours, and then Et_2O (20 mL) was added to the resulting solution to yield a blue powder, which was collected by filtration, washed with Et_2O, and dried *in vacuo*. Yield: 0.17 g (63%). UV-vis (λ_{max} (nm) [ε (M^{-1} cm^{-1})]) in CH_3CN: ~850 (500). ESI-MS in CH_3CN: *m*/*z* 167.1 for $[Cu(Me_6\text{-tren})(CH_3CN)]^{2+}$ and *m*/*z* 392.1 for $[Cu(Me_6\text{-tren})(ClO_4)]^+$. The BPh_4 salt of this complex was obtained by dissolution of this solid in CH_3CN and addition of 4 equiv of $NaBPh_4$ in CH_3CN. Vapor diffusion of Et_2O into this solution yielded blue crystals suitable for X-ray diffraction. *Caution: Perchlorate salts are potentially explosive and should be handled with care!*

UV-vis spectra were recorded on a Hewlett Packard 8453 diode array spectrophotometer equipped with a UNISOKU Scientific Instruments for low-temperature experiments or with a circulating water bath. Electrospray ionization mass spectra (ESI-MS) were collected on a Thermo Finnigan (San Jose, CA, USA) LCQ™ Advantage MAX quadrupole ion trap instrument, by infusing samples directly into the source using a manual method. The spray voltage was set at 4.2 kV and the capillary temperature at 80 °C. Resonance Raman spectra were obtained using a liquid nitrogen cooled CCD detector (CCD-1024 × 256-OPEN-1LS, HORIBA Jobin Yvon) attached to a 1-m single polychromator (MC-100DG, Ritsu Oyo Kogaku) with a holographic grating (1200 grooves mm^{-1}). Excitation wavelengths of 406.7 nm and 441.6 nm were provided by a Kr^+ laser (Spectra Physics, BeamLok 2060) and a He–Cd laser (Kimmon Koha, IK5651R-G and KR1801C), respectively, with 15 mW power at the sample point. All measurements were carried out with a spinning cell (1000 rpm) at −20 °C. Raman shifts were calibrated with indene, and the accuracy of the peak positions of the Raman bands was ±1 cm^{-1}. Product analysis was performed with an Agilent Technologies 6890 N gas chromatograph (GC) and Thermo Finnigan (Austin, Texas, USA) FOCUS DSQ (dual stage quadrupole) mass spectrometer interfaced with Finnigan FOCUS gas chromatograph (GC-MS). EPR spectra were taken at 4 K using a X-band Bruker EMX-plus spectrometer equipped with a dual-mode cavity (ER 4116DM). Low temperature was achieved and controlled with an Oxford Instruments ESR900 liquid He quartz cryostat with an Oxford Instruments ITC503 temperature and gas flow controller.

Generation and characterization of $[Cu(Me_6\text{-tren})(OOH)]^+$ (2)

Treatment of $[Cu(Me_6\text{-tren})(CH_3CN)](ClO_4)_2$ (0.4 mM) with 10 equiv H_2O_2 in the presence of 2 equiv triethylamine (TEA) in CH_3CN/CH_3OH (1:1) at 0 °C afforded a green solution. $[Cu(Me_6\text{-tren})(^{18}O^{18}OH)]^+$ was prepared by adding 10 equiv $H_2{}^{18}O_2$ (6 μL, 90% ^{18}O-enriched, 2% $H_2{}^{18}O_2$ in water) to a solution containing $[Cu(Me_6\text{-tren})(CH_3CN)](ClO_4)_2$ (0.4 mM) and 2 equiv TEA in CH_3CN/CH_3OH (1:1) at 0 °C. UV-vis (λ_{max} (nm) [ε (M^{-1} cm^{-1})]) in CH_3CN: 375 (1250), 680 (220), 840 (270). ESI-MS in CH_3CN/CH_3OH (1:1) at 0 °C: *m*/*z* 326.1 for $[Cu(Me_6\text{-tren})(OOH)]^+$.

Generation and characterization of $[Cu(Me_6\text{-tren})(OOC(CH_3)_2Ph)]^+$ (3)

Treatment of $[Cu(Me_6\text{-tren})(CH_3CN)](ClO_4)_2$ (2 mM) with 5 equiv cumene hydroperoxide (cumyl-OOH) in the presence of 2 equiv TEA in CH_3CN afforded a green solution. $[Cu(Me_6\text{-tren})(^{18}O^{18}OC(CH_3)_2Ph)]^+$ was prepared by adding 5 equiv cumyl-$^{18}O^{18}OH$ to a solution containing $[Cu(Me_6\text{-tren})(CH_3CN)](ClO_4)_2$ (0.4 mM) and 2 equiv TEA in CH_3CN at ambient temperature. UV-vis (λ_{max} (nm) [ε (M^{-1} cm^{-1})]) in CH_3CN: 440 (280), 680 (250), 737 (300). ESI-MS in CH_3CN at 25 °C: *m*/*z* 444.0 for $[Cu(Me_6\text{-tren})(OOC(CH_3)_2Ph)]^+$.

X-ray crystallography

A single crystal of $[Cu(Me_6\text{-tren})(CH_3CN)](BPh_4)_2$ (**1**-$(BPh_4)_2$) was picked from solutions by a nylon loop (Hampton Research Co.) on a hand-made copper plate mounted inside a liquid N_2 Dewar vessel at *ca.* −40 °C and mounted on a goniometer head in a N_2 cryostream. Data collections were carried out on a Bruker SMART APEX CCD equipped with a monochromator in the Mo Kα (λ = 0.71073 Å) incident beam. The CCD data were integrated and scaled using the Bruker-SAINT software package, and the structure was solved and refined using SHEXTL V 6.12.[70] Hydrogen atoms were located in the calculated positions. Crystal data for **1**-$(BPh_4)_2$: $C_{62}H_{73}B_2N_5Cu$, triclinic, $P\bar{1}$, Z = 2, a = 11.9513(17), b = 12.3535(18), c = 8.160(3) Å, α = 90.838(3), β = 91.333(3), γ = 90.275(3), V = 2680.1(7) $Å^3$, μ = 0.451 mm^{-1}, ρ_{calcd} = 1.206 g cm^{-3}, R_1 = 0.0440, wR_2 = 0.0871 for 10 297 unique reflections, 630 variables. The crystallographic data for **1**-$(BPh_4)_2$ are listed in Table 3, and Table 1 lists the selected bond distances and angles.

Computational details

The DFT calculations were done using Jaguar 7.7[71] at unrestricted B3LYP level[72–76] using LACVP basis set[71,77] as defined in Jaguar. This basis set is of double-ζ quality (6-31G) with an effective core potential on the transition metals, and is widely used for geometry optimizations. An extension of this basis set at triple-ζ quality with polarization and diffuse functions (LACV3P^{*+})[71] was used for single-point energy calculation to compare the different isomers of **3**. Due to their computationally demanding nature, the frequency calculations were done on the LACVP level. A scaling factor of 0.9613 for the calculated vibration frequencies is sometimes recommended for B3LYP due to systematic overestimation originating from inaccurately calculated electron correlation interactions as well as the harmonic approximation.[78] However, this scaling factor is based on calculations with a slightly different basis set (6-31G(d)), and in our systems, the scaling in fact gave worse agreement with the experimental results. The calculations were done in the gas-phase, and the validity of the chosen method for structural calculations was confirmed by calculating **1**, with total charge/mutiplicity set to +2/2 respectively, and compare it to the crystal structure as described in the main text. Using the same method, the structures of **2** and **3** (both +1/2) were subsequently calculated.

Reactivity

All reactions were run in a 1-cm UV cuvette by monitoring UV-vis spectral changes of reaction solutions, and rate constants were determined by fitting the changes in absorbance at 375 nm for **2** and 440 nm for **3**. Reactions were run at least in triplicate, and the data reported represent the average of these reactions. The purity of substrates was checked with GC and GC–MS prior to use. After completion of the reactions, products were analyzed by injecting reaction solutions directly into GC and GC–MS. Products were identified by comparing with authentic samples, and product yields were determined by comparison against standard curves prepared with authentic samples and using decane as an internal standard.

Supplementary Material

Refer to Web version on PubMed Central for supplementary material.

Acknowledgments

The research was supported by NRF/MEST of Korea through CRI (W.N.) and WCU (R31-2008-000-10010-0) (W.N. and K.D.K.) Programs, the Ministry of Education, Culture, Sports, Science and Technology of Japan through the Global COE program and Priority Area (No. 20050029) (T.O.), NIH grant GM-28962 (K.D.K.), and NRF (NRF-2010-1054-1-2) (J.C.).

References

1. Sheldon, RA.; Kochi, JK. Metal-Catalyzed Oxidations of Organic Compounds. Academic Press; New York: 1981.
2. Mimoun, H. The Chemistry of Functional Groups Peroxides. Patai, S., editor. Wiley; New York: 1983. p. 463-482.
3. Martell, AE.; Sawyer, DT. Oxygen Complexes and Oxygen Activation by Transition Metals. Plenum; New York: 1988.
4. Spiro, TG. Metal ion activation of dioxygen: Metal ions in biology. Wiley-interscience; New York: 1981.
5. Holm RH, Solomon EI. Chem Rev. 2004; 104:347–348. and review articles in the special issue. [PubMed: 14871127]
6. Nam W. Acc Chem Res. 2007; 40:465. and review articles in the special issue.

7. Karlin KD. Nature. 2010; 463:168–169. [PubMed: 20075910]
8. Karlin KD, Kaderli S, Zuberbühler AD. Acc Chem Res. 1997; 30:139–147.
9. Hatcher LQ, Karlin KD. Adv Inorg Chem. 2006; 58:131–184.
10. Himes RA, Karlin KD. Curr Opin Chem Biol. 2009; 13:119–131. [PubMed: 19286415]
11. Kamachi T, Lee YM, Nishimi T, Cho J, Yoshizawa K, Nam W. J Phys Chem A. 2008; 112:13102–13108. [PubMed: 18991428]
12. Solomon EI, Sundaram UM, Machonkin TE. Chem Rev. 1996; 96:2563–2605. [PubMed: 11848837]
13. Solomon EI, Chen P, Metz M, Lee SK, Palmer AE. Angew Chem, Int Ed. 2001; 40:4570–4590.
14. Mirica LM, Ottenwaelder X, Stack TDP. Chem Rev. 2004; 104:1013–1045. [PubMed: 14871148]
15. Rosenzweig AC, Sazinsky MH. Curr Opin Struct Biol. 2006; 16:729–735. [PubMed: 17011183]
16. Kosman DJ. JBIC, J Biol Inorg Chem. 2010; 15:15–28.
17. Matoba Y, Kumagai T, Yamamoto A, Yoshitsu H, Sugiyama M. J Biol Chem. 2006; 281:8981–8990. [PubMed: 16436386]
18. Solomon EI, Augustine AJ, Yoon J. Dalton Trans. 2008:3921–3932. [PubMed: 18648693]
19. Bento I, Martins LO, Lopes GG, Carrondo MA, Lindley PF. Dalton Trans. 2005:3507–3513. [PubMed: 16234932]
20. Chen Z, Durao P, Silva CS, Pereira MM, Todorovic S, Hildebrandt P, Bento I, Lindley PF, Martins LO. Dalton Trans. 2010; 39:2875–2882. [PubMed: 20200715]
21. Würtele C, Gaoutchenova E, Harms K, Holthausen MC, Sundermeyer J, Schindler S. Angew Chem, Int Ed. 2006; 45:3867–3869.
22. Maiti D, Fry HC, Woertink JS, Vance MA, Solomon EI, Karlin KD. J Am Chem Soc. 2007; 129:264–265. [PubMed: 17212392]
23. Prigge ST, Eipper BA, Mains RE, Amzel LM. Science. 2004; 304:864–867. [PubMed: 15131304]
24. Chen P, Root DE, Campochiaro C, Fujisawa K, Solomon EI. J Am Chem Soc. 2003; 125:466–474. [PubMed: 12517160]
25. Aboelella NW, Lewis EA, Reynolds AM, Brennessel WW, Cramer CJ, Tolman WB. J Am Chem Soc. 2002; 124:10660–10661. [PubMed: 12207513]
26. Wada A, Harata M, Hasegawa K, Jitsukawa K, Masuda H, Mukai M, Kitagawa T, Einaga H. Angew Chem, Int Ed. 1998; 37:798–799.
27. Ohta T, Tachiyama T, Yoshizawa K, Yamabe T, Uchida T, Kitagawa T. Inorg Chem. 2000; 39:4358–4369. [PubMed: 11196933]
28. Kodera M, Kita T, Miura I, Nakayama N, Kawata T, Kano K, Hirota S. J Am Chem Soc. 2001; 123:7715–7716. [PubMed: 11481001]
29. Fujii T, Yamaguchi S, Funahashi Y, Ozawa T, Tosha T, Kitagawa T, Masuda H. Chem Commun. 2006:4428–4430.
30. Yamaguchi S, Masuda H. Sci Technol Adv Mater. 2005; 6:34–47.
31. Maiti D, Lucas HR, Sarjeant AAN, Karlin KD. J Am Chem Soc. 2007; 129:6998–6999. [PubMed: 17497785]
32. Maiti D, Sarjeant AAN, Karlin KD. J Am Chem Soc. 2007; 129:6720–6721. [PubMed: 17474748]
33. Kunishita A, Scanlon JD, Ishimaru H, Honda K, Ogura T, Suzuki M, Cramer CJ, Itoh S. Inorg Chem. 2008; 47:8222–8232. [PubMed: 18698765]
34. Kunishita A, Kubo M, Ishimaru H, Ogura T, Sugimoto H, Itoh S. Inorg Chem. 2008; 47:12032–12039. [PubMed: 18998628]
35. Maiti D, Lee DH, Gaoutchenova K, Würtele C, Holthausen MC, Sarjeant AAN, Sundermeyer J, Schindler S, Karlin KD. Angew Chem, Int Ed. 2008; 47:82–85.
36. Maiti D, Sarjeant AAN, Karlin KD. Inorg Chem. 2008; 47:8736–8747. [PubMed: 18783212]
37. Schindler S. Eur J Inorg Chem. 2000:2311–2326.
38. Würtele C, Sander O, Lutz V, Waitz T, Tuczek F, Schindler S. J Am Chem Soc. 2009; 131:7544–7545. [PubMed: 19441813]
39. Schatz M, Becker M, Walter O, Liehr G, Schindler S. Inorg Chim Acta. 2001; 324:173–179.

40. Komiyama K, Furutachi H, Nagatomo S, Hashimoto A, Hayashi H, Fujinami S, Suzuki M, Kitagawa T. Bull Chem Soc Jpn. 2004; 77:59–72.
41. Itoh S. Curr Opin Chem Biol. 2006; 10:115–122. [PubMed: 16504568]
42. Cramer CJ, Tolman WB. Acc Chem Res. 2007; 40:601–608. [PubMed: 17458929]
43. Klinman JP. J Biol Chem. 2006; 281:3013–3016. [PubMed: 16301310]
44. Chen P, Solomon EI. Proc Natl Acad Sci U S A. 2004; 101:13105–13110. [PubMed: 15340147]
45. Kunishita A, Kubo M, Sugimoto H, Ogura T, Sato K, Takui T, Itoh S. J Am Chem Soc. 2009; 131:2788–2789. [PubMed: 19209864]
46. Poater A, Cavallo L. Inorg Chem. 2009; 48:4062–4066. [PubMed: 19331376]
47. Kitajima N, Katayama T, Fujisawa K, Iwata Y, Moro-oka Y. J Am Chem Soc. 1993; 115:7872–7873.
48. Sanyal I, Ghosh P, Karlin KD. Inorg Chem. 1995; 34:3050–3056.
49. Chen P, Fujisawa K, Solomon EI. J Am Chem Soc. 2000; 122:10177–10193.
50. Kunishita A, Teraoka J, Scanlon JD, Matsumoto T, Suzuki M, Cramer CJ, Itoh S. J Am Chem Soc. 2007; 129:7248–7249. [PubMed: 17503824]
51. Kunishita A, Ishimaru H, Nakashima S, Ogura T, Itoh S. J Am Chem Soc. 2008; 130:4244–4245. [PubMed: 18335943]
52. Yoshizawa K, Kihara N, Kamachi T, Shiota Y. Inorg Chem. 2006; 45:3034–3041. [PubMed: 16562959]
53. Gherman BF, Tolman WB, Cramer CJ. J Comput Chem. 2006; 27:1950–1961. [PubMed: 17019721]
54. Hong S, Huber SM, Gagliardi L, Cramer CC, Tolman WB. J Am Chem Soc. 2007; 129:14190–14192. [PubMed: 17958429]
55. Lee SC, Holm RH. J Am Chem Soc. 1993; 115:11789–11798.
56. The parameter τ is defined as $\tau = (\beta - \alpha)/60$, where α and β are the two largest L–M–L angles with $\beta \geq \alpha$. $\tau = 0$ for square-pyramidal and $\tau = 1$ for trigonal-bipyramidal.
57. Yamaguchi S, Wada A, Nagatomo S, Kitagawa T, Jitsukawa K, Masuda H. Chem Lett. 2004; 33:1556–1557.
58. Yamaguchi S, Nagatomo S, Kitagawa T, Funahashi Y, Ozawa T, Jitsukawa K, Masuda H. Inorg Chem. 2003; 42:6968–6970. [PubMed: 14577757]
59. Lucchese B, Humphreys KJ, Lee DH, Incarvito CD, Sommer RD, Rheingold AL, Karlin KD. Inorg Chem. 2004; 43:5987–5998. [PubMed: 15360248]
60. Karlin KD, Hayes JC, Juen S, Hutchinson JP, Zubieta J. Inorg Chem. 1982; 21:4106–4108.
61. Barbucci R, Bencini A, Gatteschi D. Inorg Chem. 1977; 16:2117–2120.
62. Jiang F, Karlin KD, Peisach J. Inorg Chem. 1993; 32:2576–2582.
63. Lee Y, Park GY, Lucas HR, Vajda PL, Kamaraj K, Vance MA, Milligan AE, Woertink JS, Siegler MA, Sarjeant AAN, Zakharov LN, Rheingold AL, Solomon EI, Karlin KD. Inorg Chem. 2009; 48:11297–11309. [PubMed: 19886646]
64. Namuswe F, Hayashi T, Jiang Y, Kasper GD, Sarjeant AAN, Moënne-Loccoz P, Goldberg DP. J Am Chem Soc. 2010; 132:157–167. [PubMed: 20000711]
65. Kohn W, Sham LJ. Phys Rev. 1965; 140:A1133–A1138.
66. Shaik S, Kumar D, de Visser SP, Altun A, Thiel W. Chem Rev. 2005; 105:2279–2328. [PubMed: 15941215]
67. Armarego, WLF.; Perrin, DD. Purification of Laboratory Chemicals. Pergamon Press; Oxford: 1997.
68. Finn MG, Sharpless KB. J Am Chem Soc. 1991; 113:113–126.
69. Britovsek GJP, England J, White AJP. Inorg Chem. 2005; 44:8125–8134. [PubMed: 16241163]
70. Sheldrick, GM. SHELXTL/PC Version 6.12 for Windows XP. Bruker AXS Inc; Madison, WI: 2001.
71. Jaguar, version 7.7. Schrödinger, LLC; New York, NY: 2010.
72. Becke AD. Phys Rev A: At, Mol, Opt Phys. 1988; 38:3098–3100.

73. Becke AD. J Chem Phys. 1993; 98:1372–1377.
74. Becke AD. J Chem Phys. 1993; 98:5648–5652.
75. Lee C, Yang W, Parr RG. Phys Rev B. 1988; 37:785–789.
76. Perdew JP. Phys Rev B. 1986; 33:8822–8824.
77. Hay PJ, Wadt WR. J Chem Phys. 1985; 82:299–310.
78. Wong MW. Chem Phys Lett. 1996; 256:391–399.

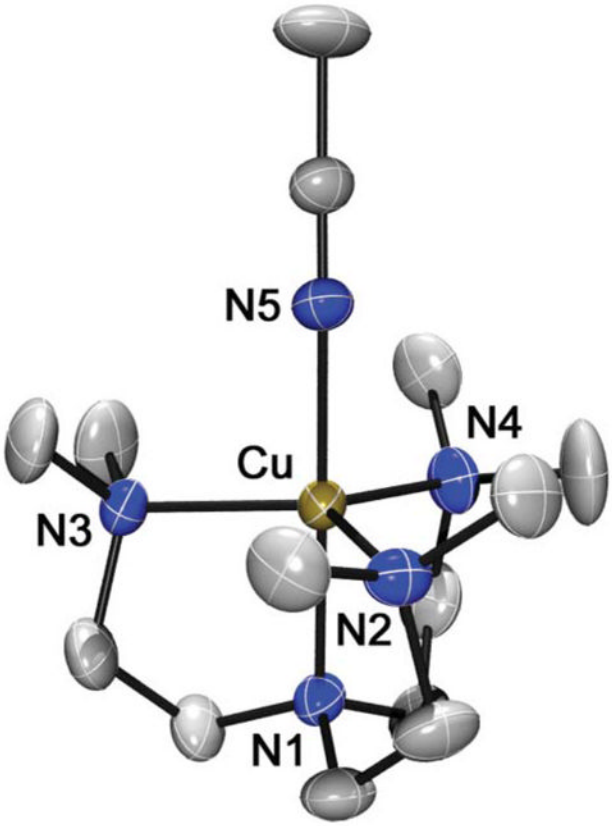

Fig. 1.
X-ray structure of the $[Cu(Me_6\text{-tren})(CH_3CN)]^{2+}$ cation in **1**-$(BPh_4)_2$ showing 30% probability thermal ellipsoids. Hydrogen atoms are omitted for clarity.

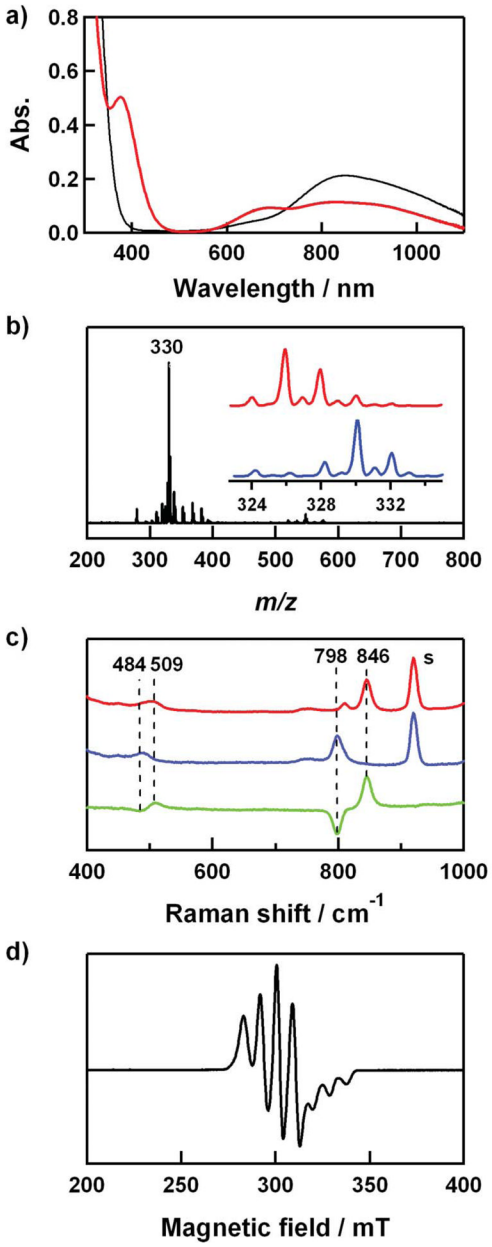

Fig. 2.

(a) UV-vis spectra of **1** (0.4 mM) (black line) and **2** (0.4 mM) (red line) in CH_3CN/CH_3OH (1:1) at 0 °C. (b) ESI-MS of **2**-^{18}O. Inset shows isotope distribution patterns for **2**-^{18}O (blue line) and **2**-^{16}O (red line). (c) Resonance Raman spectra of **2** (4 mM) obtained upon excitation at 407 nm in CH_3CN/CH_3OH (1:1) at −20 °C. Red/blue lines: samples prepared with $H_2{}^{16}O_2/H_2{}^{18}O_2$; green line: difference spectrum, (^{16}O–^{18}O). The peak marked with "s" is ascribed to the solvents. (d) X-band EPR spectrum of **2** recorded in CH_3CN/CH_3OH (1:1) at 4.3 K. Spectroscopic settings: frequency = 9.10 GHz, microwave power = 1 mW, modulation frequency = 100 kHz.

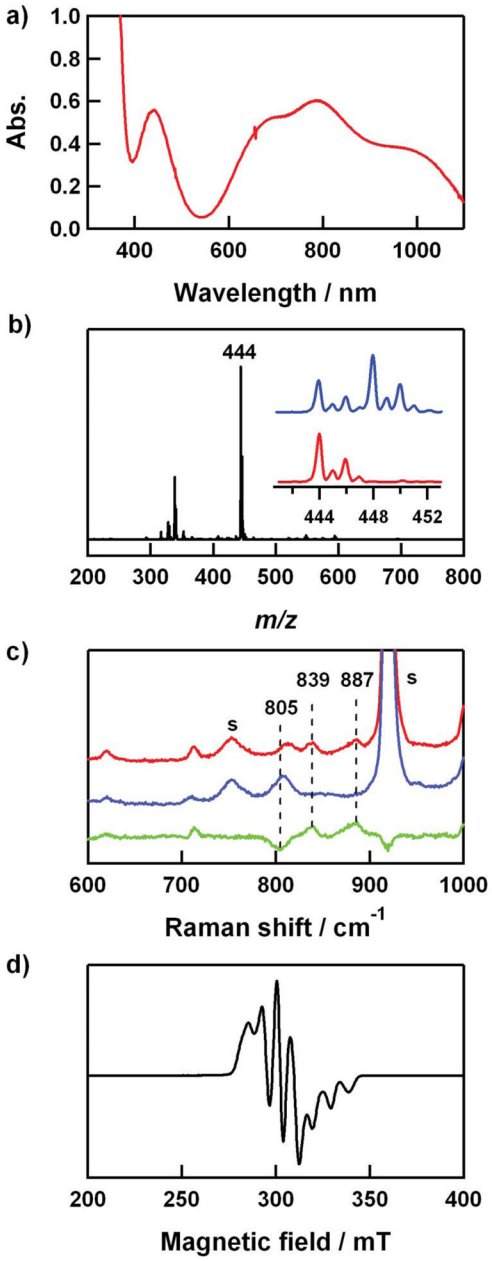

Fig. 3.

(a) UV-vis spectrum of **3** (2 mM) in CH_3CN at 25 °C. (b) ESI-MS of **3**-^{16}O. Inset shows isotope distribution patterns for **3**-^{16}O (red line) and **3**-^{18}O (blue line). Isotopically labeled cumyl-$^{18}O^{18}OH$ (70% ^{18}O-enriched) was used for **3**-^{18}O. (c) Resonance Raman spectra of **3** (16 mM) obtained upon excitation at 442 nm in CH_3CN at −20 °C. Red/blue lines were obtained with samples prepared with cumyl-$^{16}O^{16}OH$/Cumyl-$^{18}O^{18}OH$ (90% ^{18}O-enriched); green line: difference spectrum, (^{16}O – ^{18}O). The peaks marked with “s” are ascribed to the solvent. (d) X-band EPR spectrum of **3** recorded in CH_3CN at 4.3 K. Spectroscopic settings: frequency = 9.10 GHz, microwave power = 1 mW, modulation frequency = 100 kHz.

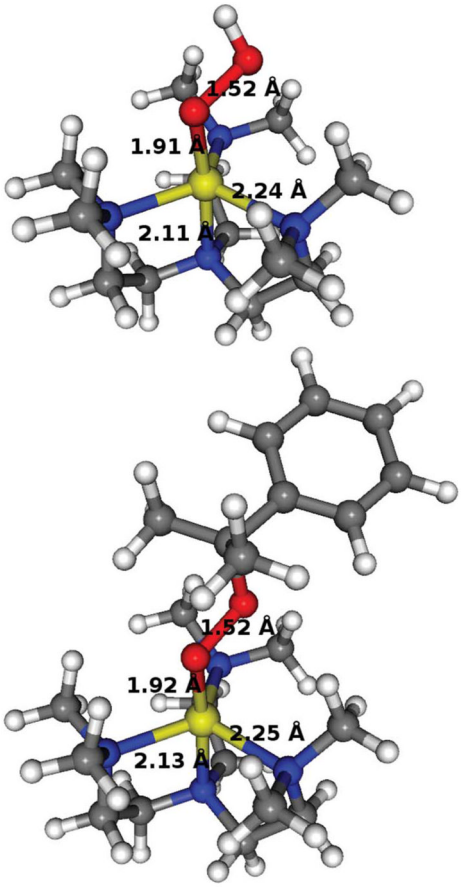

Fig. 4.

DFT calculated structures for **2** (top) and one of the isomers of **3a** (bottom) with the bond distances shown for the Cu–O, O–O, Cu–N_{ax} and (largest) Cu–N_{eq} bonds (gray, C; white, H; red, O; blue, N; yellow, Cu).

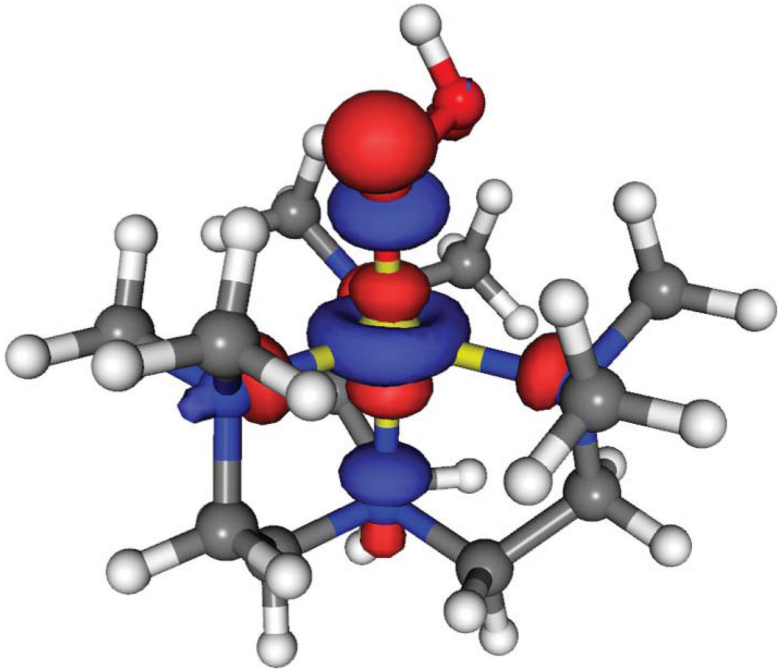

Fig. 5.
The singly occupied molecular orbital (SOMO) for **2** (and also for **3**) is a $\sigma^*_{z^2}$ orbital.

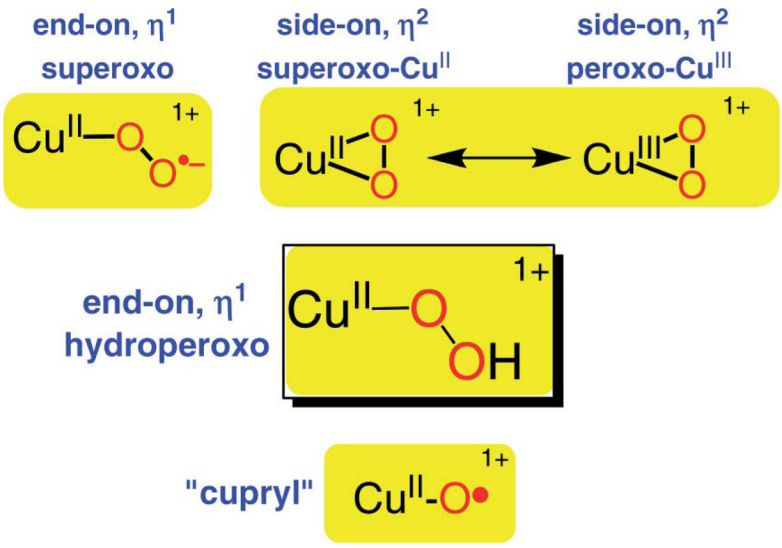

Scheme 1.
Mononuclear copper–O_2 adducts and derived species of interest.

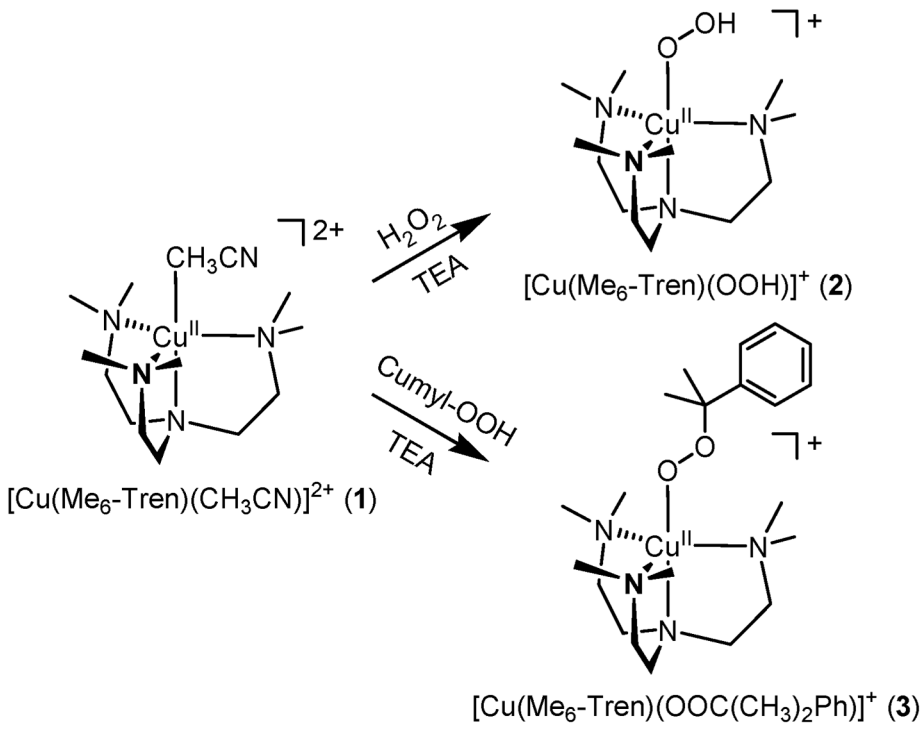

Scheme 2.

Table 1

Selected bond distances (Å) and angles (°) from the obtained crystal structure and the DFT calculations as described in the text

	Exp.	Calcd		Exp.	Calcd
Cu–N1	1.995(2)	2.07	Cu–N2	2.128(2)	2.21
Cu–N3	2.124(2)	2.22	Cu–N4	2.152(2)	2.23
Cu–N5	1.968(2)	2.05			
N1–Cu–N2	86.35(9)	85.24	N1–Cu–N3	85.36(9)	85.09
N1–Cu–N4	85.89(10)	85.02	N1–Cu–N5	178.22(11)	179.62
N2–Cu–N3	121.25(10)	119.61	N2–Cu–N4	117.40(10)	119.42
N2–Cu–N5	95.43(10)	95.13	N3–Cu–N4	119.81(10)	118.83
N3–Cu–N5	93.71(9)	94.80	N4–Cu–N5	93.27(10)	94.72

Table 2

Mulliken spin density distribution

Complex	Cu	O_{inner}	O_{outer}	4 × N	Rest
1	0.53	—	—	0.43	0.05
2	0.51	0.25	0.00	0.24	0.00
3a	0.51	0.26	−0.01	0.23	0.01

Table 3

Crystal data and structure refinements for **1**-$(BPh_4)_2$

	1-$(BPh_4)_2$
Empirical formula	$C_{62}\ H_{73}\ B_2\ CuN_5$
Formular weight	973.41
Temperature (K)	298(2)
Wavelength (Å)	0.71073
Crystal system, space group	Triclinic, $P\bar{1}$
a (Å)	11.9513(17)
b (Å)	12.3535(18)
c (Å)	18.160(3)
α (°)	90.838(3)
β (°)	91.333(3)
γ (°)	90.275(3)
Volume (Å^3)	2680.1(7)
Z	2
Calculated density (g cm^{-3})	1.206
Absorption coefficient (mm^{-1})	0.451
Reflections collected	15 072
Independent reflections [*R*(int)]	10 297 [0.0367]
Refinement method	Full-matrix least-squares on F^2
Data/restraints/parameters	10297/0/638
Goodness-of-fit on F^2	0.735
Final *R* indices [$I > 2\sigma(I)$]	$R_1 = 0.0440$, $wR_2 = 0.0803$
Largest difference peak and hole (e Å^{-3})	0.269 and −0.341